Article

Combination of a Nondestructive Testing Method with Artificial Neural Network for Determining Thickness of Aluminum Sheets Regardless of Alloy's Type

Abdulilah Mohammad Mayet [1], Muhammad Umer Hameed Shah [2,*], Robert Hanus [3], Hassen Loukil [1], Muneer Parayangat [1], Mohammed Abdul Muqeet [1], Ehsan Eftekhari-Zadeh [4,*] and Ramy Mohammed Aiesh Qaisi [5]

[1] Electrical Engineering Department, King Khalid University, Abha 61411, Saudi Arabia; amayet@kku.edu.sa (A.M.M.); hloukil@kku.edu.sa (H.L.); mparayangat@kku.edu.sa (M.P.); mabdulmuqeet@kku.edu.sa (M.A.M.)

[2] Department of Mechanical Engineering and Artificial Intelligence Research Center, College of Engineering and Information Technology, Ajman University, Ajman 346, United Arab Emirates

[3] Faculty of Electrical and Computer Engineering, Rzeszów University of Technology, 35-959 Rzeszów, Poland; rohan@prz.edu.pl

[4] Institute of Optics and Quantum Electronics, Friedrich Schiller University Jena, Max-Wien-Platz 1, 07743 Jena, Germany

[5] Department of Electrical and Electronics Engineering, College of Engineering, University of Jeddah, Jeddah 21589, Saudi Arabia; dgaisi@uj.edu.sa

* Correspondence: m.shah@ajman.ac.ae (M.U.H.S.); e.eftekharizadeh@uni-jena.de (E.E.-Z.)

Abstract: Non-destructive and reliable radiation-based gauges have been routinely used in industry to determine the thickness of metal layers. When the material's composition is understood in advance, only then can the standard radiation thickness meter be relied upon. Errors in thickness measurements are to be expected in settings where the actual composition of the material may deviate significantly from the nominal composition, such as rolled metal manufacturers. In this research, an X-ray-based system is proposed to determine the thickness of an aluminum sheet regardless of its alloy type. In the presented detection system, an X-ray tube with a voltage of 150 kV and two sodium iodide detectors, a transmission detector and a backscattering detector, were used. Between the X-ray tube and the transmission detector, an aluminum plate with different thicknesses, ranging from 2 to 45 mm, and with four alloys named 1050, 3050, 5052, and 6061 were simulated. The MCNP code was used as a very powerful platform in the implementation of radiation-based systems in this research to simulate the detection structure and the spectra recorded using the detectors. From the spectra recorded using two detectors, three features of the total count of both detectors and the maximum value of the transmission detector were extracted. These characteristics were applied to the inputs of an RBF neural network to obtain the relationship between the inputs and the thickness of the aluminum plate. The trained neural network was able to determine the thickness of the aluminum with an MRE of 2.11%. Although the presented methodology is used to determine the thickness of the aluminum plate independent of the type of alloy, it can be used to determine the thickness of other metals as well.

Keywords: nondestructive testing; aluminum plate; thickness meter; RBF neural network; X-ray-based detection system; alloy

1. Introduction

Despite the fact that they cannot precisely determine the metal thickness with a high surface roughness and require a connection between the measuring tool and a moving sheet of metal [1], contact thickness measures are generally reliable and can operate regardless of the temperature of the metal. Metal sheet thickness has been measured using radiation

gauges for quite some time. Radiation sources and detectors, which are on the opposite ends of the sheet, make up the bulk of a radiation thickness gauge. By specifying the material's composition, a conventional radiation thickness meter may work correctly, as stated by Lambert–Beer law, which suggests that photon attenuation is a consequence of either the thickness of matter or its chemical makeup. Errors in thickness measurements are to be expected in settings where the actual composition of the material may deviate significantly from the standard composition or the nominal, such as in rolled metal manufacturers [2]. If reliable measurements of the thickness of different alloys are to be collected, the circumstances described above require the use of a traditional thickness gauge that is based on gamma radiation and requires periodic calibration. The principal disadvantages of continuous calibrations are the time required for each calibration procedure and the necessity of many reference samples of each kind of alloy. Some studies on the non-calibrated thickness measurement of metal sheets of different alloys have been conducted in recent years. Research [2] put out an idea for a theoretical procedure that may be used to determine the thickness of a variety of alloy sheets. They used two detectors and two radiation sources of varied energies, such as two X-ray tubes of varying voltages, one X-ray tube and one gamma ray emitter source, or two gamma ray emitter sources of various energies. They were able to detect a change in the composition of the sheet by analyzing the difference in the ratio of coefficients of attenuation (μ) at the two energies. When they conducted this analysis, they applauded their discovery. Changes in the ratio of the coefficient may be used to modify results from two-energy-source thickness measurements. Rolling non-ferrous metals into components of varying thicknesses, Artem'ev et al. [1] advocated using an X-ray thickness meter in 2003 so that they could account for variations in the alloy composition while making their measurements. An ionization chamber and an X-ray tube were among their tools. Samples of copper alloys with varied thicknesses were ionized, and the resulting signals were recorded. After giving the data that were associated with a single alloy type as a reference, the team supplied a formulaic correction function that was based on the value of reference in order to account for the influence that different alloy compositions had on thickness measurement. While this approach helped to decrease systematic error in measurements, the mathematical correction factor they used only applied to a single alloy and hence was not suitable for online measurements of a wider variety of metals. References [3,4] expand on the work of the aforementioned writers on the subject of metal thickness meters. A straightforward and intelligent gamma-ray-based system that makes use of AI was reported in [5] for the purpose of online thickness measuring of metal sheets made of a variety of alloys. Aluminum sheets were the focus of the research in this article. First, the MCNPX code was used to look at how well different configurations of the two detection methods (dual energy and dual modality) worked so that the best configuration for each could be found. Then, an experimental structure was made using the efficient method found via simulations. Eventually, an ANN model was built and put into use for gauging the thickness of aluminum sheets of varying compositions. X-ray tubes are very popular among writers owing to their many benefits. X-ray tubes provide many benefits over other types of sources, such as radioisotopes, which are discussed below. The X-ray tube has the potential to alter the energy of the photons released by radioisotopes, even if this energy does not vary. Although it is common knowledge that radioisotopes lose their useful qualities with time, this is not the case with an X-ray tube. For the sake of the individuals utilizing these equipment, having a way to turn the X-ray tube on and off is essential. It is easier to carry them than radioactive materials [6–9].

This study employed an X-ray tube to determine the thickness of an aluminum plate regardless of the alloy it was made of, providing a solution to the issues associated with employing radioisotopes. In the introduced system, there is an X-ray tube and two detectors; one of the detectors is responsible for recording transmission photons and the other is responsible for recording backscattering photons. In order to better interpret the data, reduce the volume of calculations, and increase the accuracy of the presented system, three characteristics of the spectra recorded using the detectors were recorded and applied to the

inputs of the neural network. The RBF neural network was responsible for determining the thickness of aluminum plates. The steps of the current research are as follows: 1. The structure of the thickness measurement system will be provided in detail. 2. The recorded signals will be analyzed and processed, and appropriate characteristics will be extracted from the signals. 3. An RBF neural network will be trained using the extracted features. 4. The neural network results will be analyzed.

2. Simulation Setup

To kick off this inquiry, a model of the detecting system structure to determine the thickness of aluminum layers of varied alloys was created in the Monte Carlo N-Particle X version (MCNPX) software. The MCNPX algorithm is an effective resource for modeling the propagation of many types of radiation (neutrons, gamma rays, electrons, etc.) [10]. Gamma/X-ray radiation-based measuring gauges [11–13], radiation shielding [14–16], industrial imaging systems [17–19], etc., have all been evaluated using the MCNPX code in recent years for their performance. In this research, aluminum was investigated in four different alloys named 1050, 3105, 5052, and 6061 in 23 different thicknesses from 2 mm to 45 mm. Densities of 2.73, 2.71, 2.7, and 2.68 g/cm^3 were found for the alloys 3105, 1050, 6061, and 5052 that were used to stand in for the aluminum sheet. Density and alloy type were selected for the simulations based on what sheets were currently accessible in the lab, bringing the practical results closer to the predictions. The proposed thickness gauge structure includes an X-ray tube, activated at a voltage of 150 kV, as a source and two sodium iodide detectors. One of the detectors is placed exactly in front of the source at a distance of 420 mm from it to record the transmitted photons. Another detector is placed next to the source at an angle of 45 degrees to the direction of X-ray emission to record the backscattered photons. In this simulation, the test aluminum plates in this simulation were positioned 140 mm from the light source. The detector was a cylindrical container containing NaI with a density of 3.67 g/cm^3; its dimensions were 7.62 cm (three inches) in length and diameter. We counted pulses using the F8 setting. For a more accurate simulation of the entire spectrum in the detector, the MCNPX approach may use an extra card of tally F8, aptly dubbed FT8 GEB, that accounts for the Gaussian energy broadening of the current detector in the laboratory. The values of a, b, and c listed on this card are experimental parameters. Similar to the prior work [20], this study made use of the GEB card in order to calculate the necessary a, b, and c parameters. This work proposes a more feasible geometry for modeling a whole industrial X-ray tube using the MCNPX code by replacing the traditional cathode (electron source) and anode (tungsten target) inside a cylindrical housing with a photon source housed within a metal shield. Since photon tracking in the MCNPX code is substantially quicker than electron tracking, only a photon source embedded in a metal shield was investigated in the present inquiry instead of modeling the cathode-anode buildup. Hernandez et al. [21] showed how to utilize the open-source program TASMIC to determine the X-ray energy spectrum and to describe the light source. Radiation shields for X-ray tubes, which are typically cylindrical in form, are composed of steel or lead. The output window is an opening in the shield surface through which naturally occurring X-ray photons may escape. In this investigation, the simulated X-ray's output window has a 5 cm radius. A 2.5 mm thick aluminum filter was inserted in front of the output window to filter the low energy photons and reduce scattering. Ninety-two different aluminum plates (4 types of alloys × 23 thicknesses) were examined in the provided thickness detection system. The data recorded using the detectors were collected and labeled. The structure of the thickness detection system simulated by the MCNP code can be seen in Figure 1. The spectra recorded using the transmission detector for different aluminum plate thicknesses are shown in Figure 2. The signals recorded using the detectors have many dimensions, and their interpretation is very difficult. On the other hand, the large volume of these data increases the volume of calculations applied to the system. To solve this problem, we want to feature extraction techniques. Two characteristics were extracted from the transmission detector with the names of total count and maximum value,

and one characteristic with the name of total count was extracted from the backscattering detector. The extracted characteristics according to the thickness of the aluminum plate and its type of alloy are shown in Figure 3. As is clear in this figure, the extracted features are able to provide acceptable separability for the thicknesses of the aluminum plate; for this purpose, these features have been used as the inputs of the neural network. The RBF neural network will try to determine the thickness of the aluminum plate using the introduced characteristics. In the next section, the description of the RBF neural network is provided in detail.
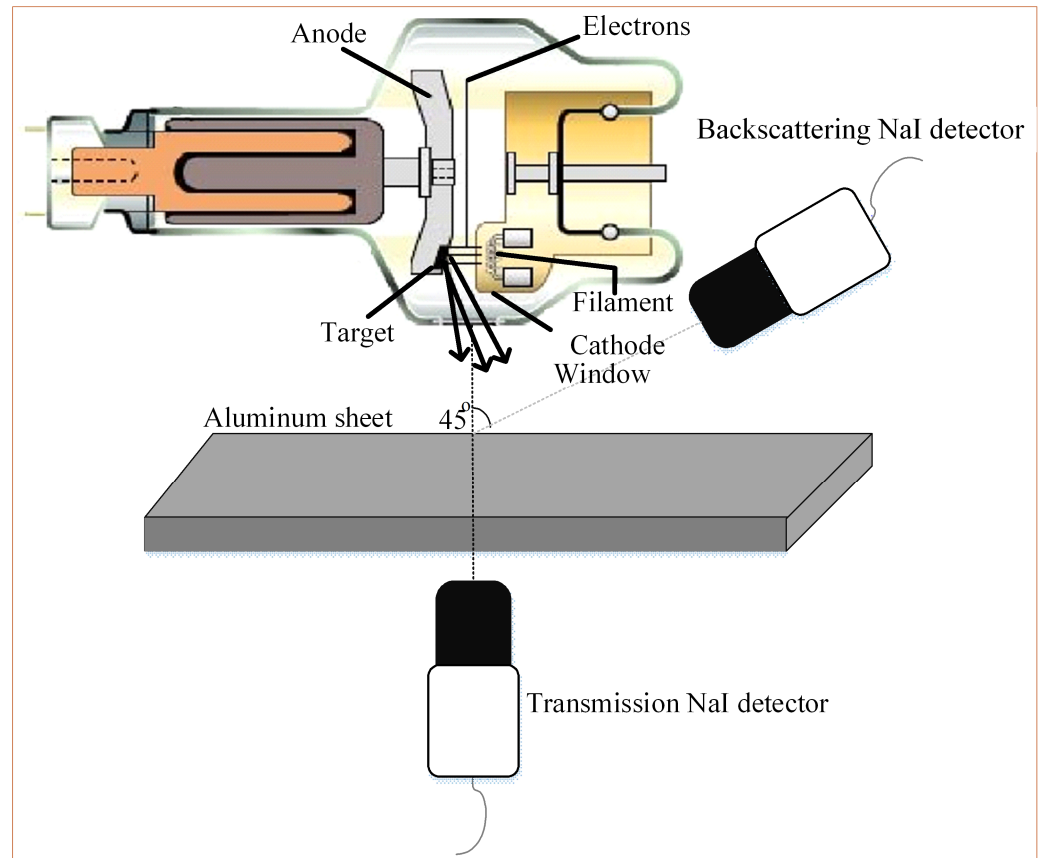

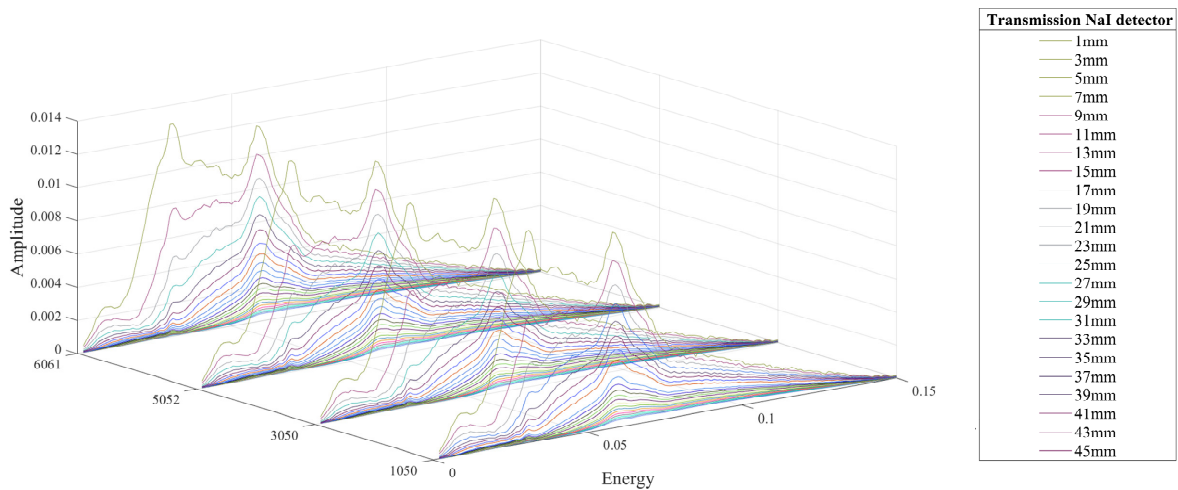**Figure 1.** System architecture for measuring thickness.

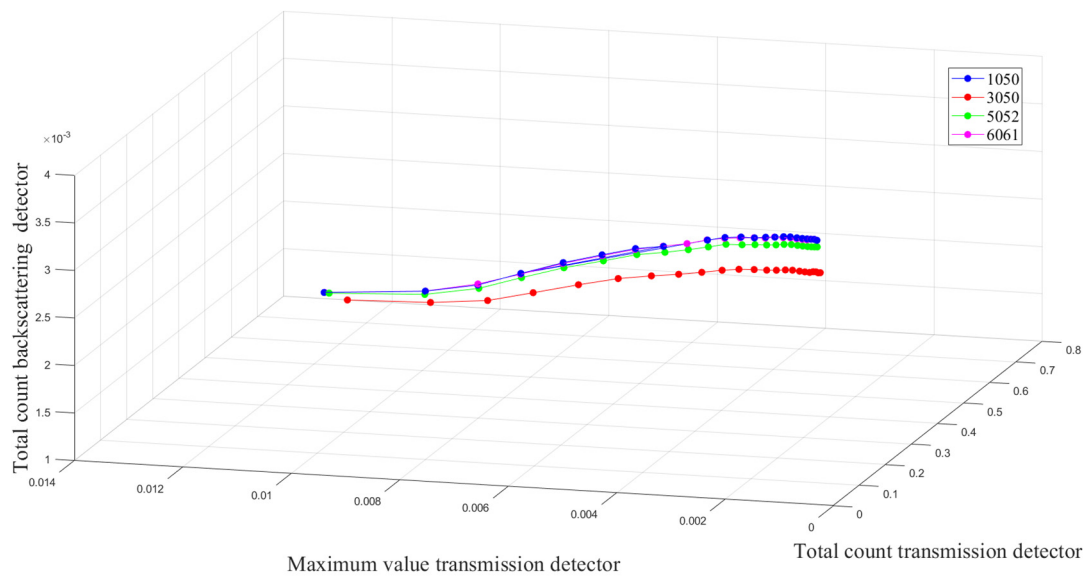**Figure 2.** Recorded spectra using transmission detector.

Figure 3. Extracted features in terms of the aluminum thickness and alloy type.

3. RBF Neural Network

Researchers in a wide variety of disciplines, including electronics [22], oil and petro-chemicals [23,24], agricultural engineering [25,26], etc., have been interested in neural networks due to their potential as useful tools. In the mentioned research, different neural networks, different feature extraction methods, and different machine learning algorithms have been used in different fields, which can inspire further research. Many scientists have employed artificial neural networks to calculate a wide range of parameters. The RBF neural network is widely used because it learns quickly and efficiently. The activation function of this neural network is a radial basis function. In addition, there are just three layers in this feed-forward type network [27–29]. Since it is a linear layer, the input layer's only function is to evenly disperse the inputs. The second layer uses the Gaussian function to create a non-linear layer. Final outputs are a linear mixture of Gaussian distributions. Since this neural network learns quickly, it may be used in real-time settings. The RBF neural network's second-layer radial basis function is represented by Equation (1) [29]:

$$\varphi(r) = \exp\left[-\frac{r^2}{2\sigma^2}\right] \tag{1}$$

where r represents a distance from the cluster's center and σ represents the breadth of the bell curve. The second layer contains computer units called hidden nodes. Central to each hidden node is a parametric vector c, whose length is proportional to that of the input vector x. The formula for determining the Euclidean distance between points c and x is as follows (Equation (2)).

$$r_j = \sqrt{\sum_{i=1}^{n}(x_i - w_{ij})^2} \tag{2}$$

The hidden layer's jth neuron output is calculated using Equation (3).

$$\varnothing_j = \exp\left[-\frac{\sum_{i=1}^{n}(x_i - w_{ij})^2}{2\sigma^2}\right] \tag{3}$$

w_{ij} stands for the weights. Traditional approaches, such as the K-Mean algorithm [30] or methods based on the Kohonen algorithm [31], may be used to obtain weights. However, supervised training is used; the number of expected clusters (k) is selected in advance, and the best fit is obtained using these techniques. When putting together a neural network, the information is first divided into two categories: training data and test data. The training

data are used to create a neural network, with the various retinal parameters tuned to minimize error. After the training process is complete, the network's performance should be assessed with data it has never seen before. If a network makes it this far, it will be able to function properly under real-world situations. In this study, the neural network was trained and its parameters optimized using around 70% of the available data, while the remaining data were used as input during the assessment phase. The RBF neural network was trained and tested in MATLAB 9.5 R2018a for this study. Although there are several pre-designed toolboxes in this software for training various neural networks, none were utilized in this study. Instead, each step was carefully programmed from scratch. The neural network was trained using the characteristics of the total count of both detectors and the maximum value of the transmission detector as inputs, and the thickness of the aluminum layer as the output. In an iterative process, we tested several configurations of the hidden layer's neurons until we found one that produced the fewest errors on both the test data and the training data. It is important to tailor your optimization strategy to the specifics of your data, which is why there are many different approaches. In this study, the inputs and output data were transformed to lie within the interval [0, 1], and once the network was trained, the transformed data were restored to their original values.

4. Results

In this research, an RBF neural network was trained to detect the thickness of the aluminum layer. This neural network used the total count of both detectors and the maximum value of the transmission detector as inputs. The network's output was the aluminum layer's thickness in mm. The neural network was implemented after simulations of different states of the aluminum layer by MCNP code. There were three neurons in the input layer, ten in the hidden layer, and one in the output layer of the trained network. After training and evaluating a variety of neural networks having anywhere from five to thirty hidden neurons, it was determined that the newly introduced structure provided the maximum accuracy. Table 1 shows the results from the evaluation of various RBF networks from 5 to 30 neurons. As is clear from this table, with the low number of neurons, the error of the training data is very high, which indicates that the neural network is not trained well. Also, with the increase in the number of neurons, the error of the training data decreases, but the error of the test data increases sharply, which shows that with the increase in the number of neurons, the network has moved towards overfitting. Using 10 neurons in the hidden layer has reduced the error of both training and testing data to an acceptable amount, so this structure was introduced as the optimal structure. Figure 4 depicts the organizational framework of this network. Table 2 displays the network's specific features. As was discussed before, the available data were separated into training and testing sets. The division of these data is completely random so that the neural network can be trained and tested from all data dispersions. Of the 92 available data, 64 were assigned to the training section, and 28 were used for the final test. The division of training and test data is completely random. The performance of the trained neural network was displayed graphically with two regression and error graphs (Figure 5). A black line and purple circles represent the regression plot. The black line shows the desired output, and the purple circles are the outputs of the neural network. The closer they are, the better the trained neural network will be. For each data point, the error graph displays the deviation from the target output that was produced by the neural network. In order to calculate the error rate of the neural network, three error parameters named mean relative error percentages (MRE%), root mean square error (RMSE), and mean absolute error (MAE) were calculated using equations 4 to 6. The RMSE calculates the average deviation between the values that a statistical model predicts and the actual values. It is the residuals' standard deviation in mathematics. The difference between the regression line and the data points is represented by residuals. The ratio of the measurement's absolute error to the actual measurement is known as the relative error. Using this technique, we can calculate the absolute error's size in terms of the measurement's actual size. The difference between the predicted value and

the actual value, expressed as an absolute number, is the absolute error. The MAE tells us how much of an error we can typically anticipate from the forecast.

$$MRE\% = 100 \times \frac{1}{N}\sum_{j=1}^{N} \left| \frac{X_j(Exp) - X_j(Pred)}{X_j(Pred)} \right| \tag{4}$$

$$RMSE = \left[\frac{\sum_{j=1}^{N} \left(X_j(Exp) - X_j(Pred) \right)^2}{N} \right]^{0.5} \tag{5}$$

$$MAE\% = \frac{1}{N}\sum_{j=1}^{N} \left| X_j(Exp) - X_j(Pred) \right| \tag{6}$$

Table 1. Results from the evaluation of various RBF networks from 5 to 30 neurons.

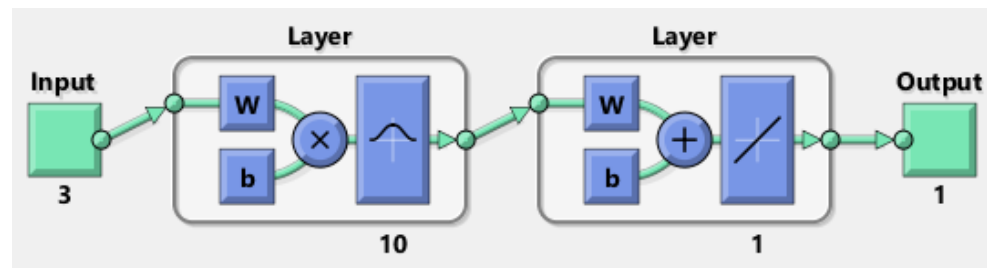| The Number of Hidden Layer Neurons	RMSE Train	RMSE Test
5	5.18	8.18
6	4.27	4.29
7	3.22	2.18
8	1.72	2.19
9	0.95	1.01
10	0.252	0.25
11	0.20	0.51
12	0.18	0.68
13	0.15	0.66
14	0.13	0.91
15	0.13	1.98
16	0.11	3.89
17	0.10	4.05
18	0.098	6.19
19	0.092	8.95
20	0.091	8.52
21	0.086	10.99
22	0.081	10.55
23	0.080	12.15
24	0.076	12.56
25	0.070	19.55
26	0.064	19.80
127	0.062	19.85
28	0.052	19.66
29	0.051	20.22
30	0.050	18.55

Figure 4. RBF neural network architecture after training.

Table 2. The specifications of the implemented neural network.

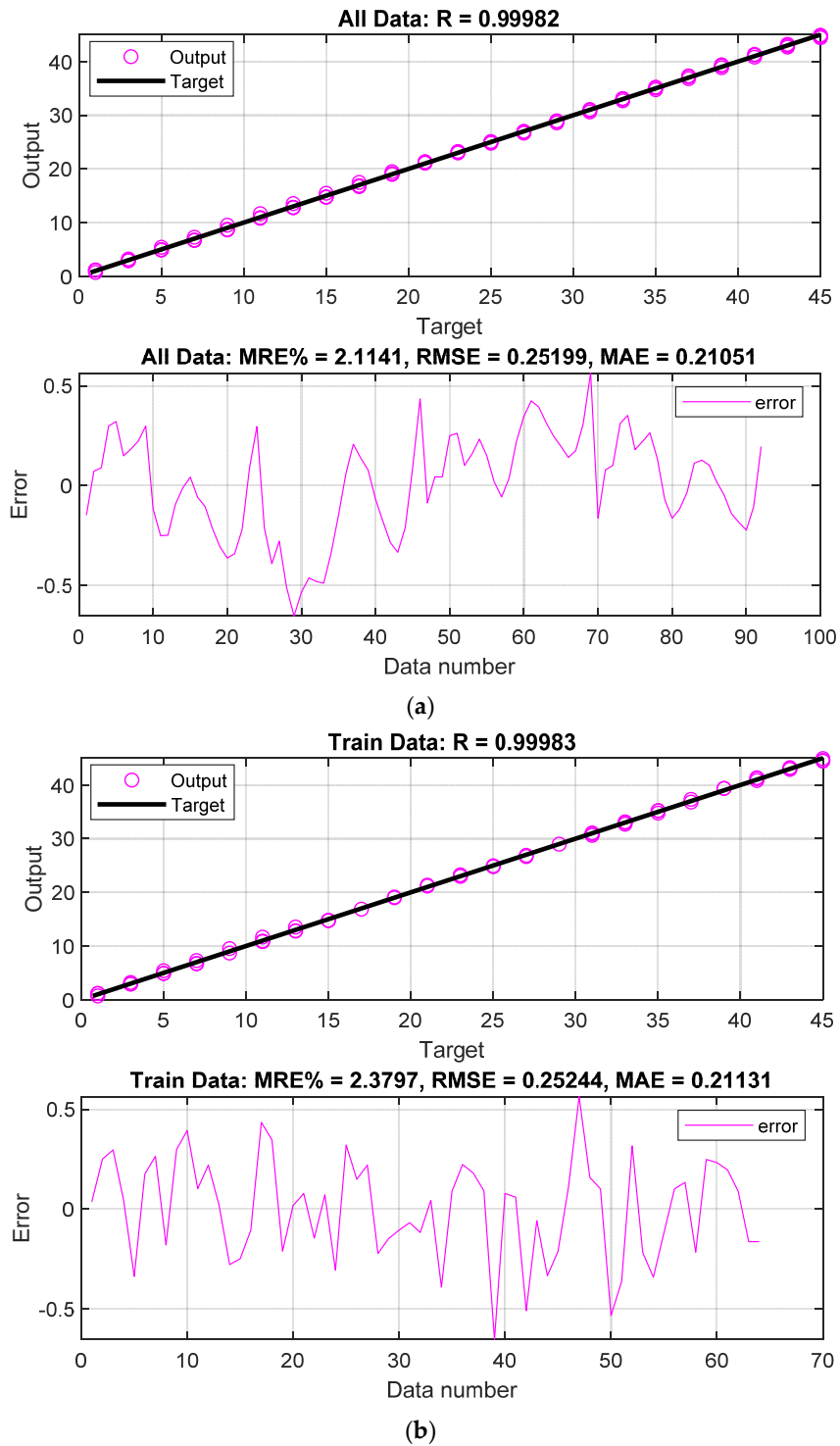| Type of Neural Network	RBF
Goal if MSE	0
Spread	0.1
MATLAB function	newrb
Input neurons	3
Hidden neurons	10
Output neuron	1

(**a**)
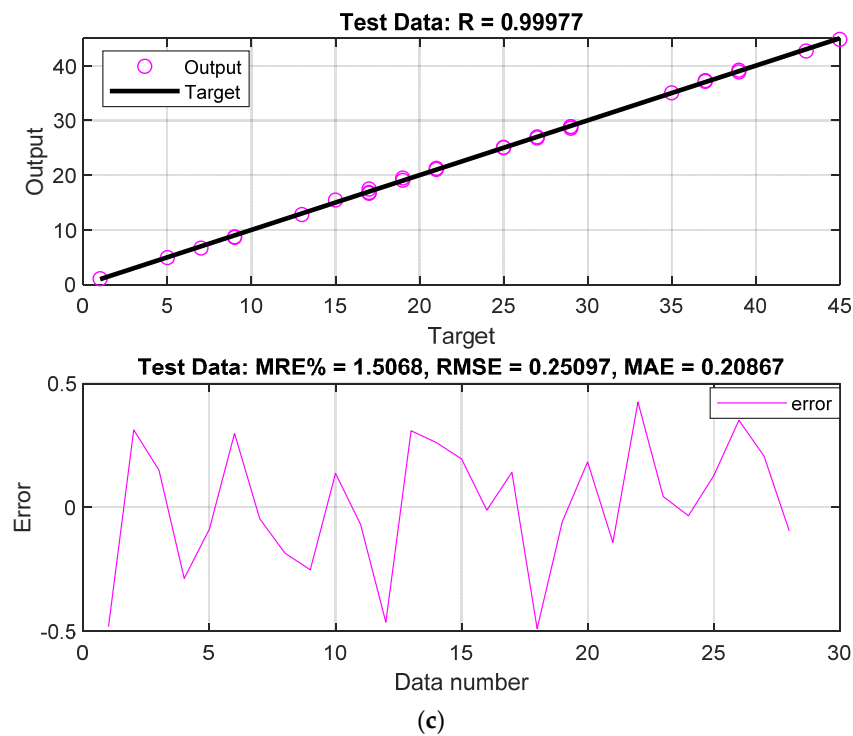

(**b**)

Figure 5. *Cont*.

Figure 5. Regression and error diagram for (**a**) all data, (**b**) train data, and (**c**) test data.

N is the number of observations, X (Exp) and X (Pred) are the experimental and projected (ANN) values, respectively. The calculated error parameters for all data—training data and test data—can be seen separately in Table 2. As is clear in this table, the neural network was able to calculate the thickness of the aluminum layer independent of the type of alloy with an MRE of 2.11%, which is considered to be a suitable and high accuracy. The neural network's input data, target output, output calculated by the neural network, and network error are shown in Tables 3 and 4.

Table 3. Calculated error parameters.

MRE% of all data	2.11%
RMSE of all data	0.25
MAE of all data	0.21
MRE% of train data	2.37%
RMSE of train data	0.25
MAE of train data	0.21
MRE% of test data	1.50%
RMSE of test data	0.25
MAE of test data	0.20

Table 4. The neural network's input data, target output, output calculated by the neural network, and network error.

Item	Total Count of Transmission Detector	Total Count of Backscatter Detector	Maximum Value of Transmission Detector	Target Outputs (mm)	Outputs of Neural Network (mm)	Error	Type of Alloy
1	0.7069	0.0013	0.0128	1	1.1483	−0.1483	1050
2	0.5339	0.0018	0.0101	3	2.9282	0.0718	1050
3	0.4297	0.0021	0.0086	5	4.9103	0.0897	1050
4	0.3563	0.0024	0.0075	7	6.7012	0.2988	1050
5	0.3002	0.0027	0.0064	9	8.6789	0.3211	1050
6	0.2559	0.0029	0.0055	11	10.8508	0.1492	1050

Table 4. *Cont.*

Item	Total Count of Transmission Detector	Total Count of Backscatter Detector	Maximum Value of Transmission Detector	Target Outputs (mm)	Outputs of Neural Network (mm)	Error	Type of Alloy
7	0.2200	0.0031	0.0047	13	12.8167	0.1833	1050
8	0.1903	0.0032	0.0040	15	14.7766	0.2234	1050
9	0.3563	0.0024	0.0075	17	16.7012	0.2988	1050
10	0.1446	0.0034	0.0030	19	19.1190	−0.1190	1050
11	0.1268	0.0035	0.0026	21	21.2518	−0.2518	1050
12	0.1116	0.0035	0.0022	23	23.2491	−0.2491	1050
13	0.0985	0.0035	0.0019	25	25.0947	−0.0947	1050
14	0.0871	0.0036	0.0017	27	27.0110	−0.0110	1050
15	0.0772	0.0036	0.0014	29	28.9580	0.0420	1050
16	0.0686	0.0036	0.0013	31	31.0588	−0.0588	1050
17	0.0611	0.0037	0.0011	33	33.1052	−0.1052	1050
18	0.0545	0.0037	0.0009	35	35.2162	−0.2162	1050
19	0.0486	0.0037	0.0008	37	37.3066	−0.3066	1050
20	0.0435	0.0037	0.0007	39	39.3638	−0.3638	1050
21	0.0390	0.0037	0.0006	41	41.3416	−0.3416	1050
22	0.0349	0.0037	0.0005	43	43.2192	−0.2192	1050
23	0.0314	0.0037	0.0005	45	44.9082	0.0918	1050
24	0.6922	0.0013	0.0123	1	0.7035	0.2965	3105
25	0.5143	0.0017	0.0099	3	3.2125	−0.2125	3105
26	0.4094	0.0020	0.0083	5	5.3920	−0.3920	3105
27	0.3367	0.0023	0.0072	7	7.2782	−0.2782	3105
28	0.2818	0.0025	0.0061	9	9.5102	−0.5102	3105
29	0.2387	0.0027	0.0051	11	11.6542	−0.6542	3105
30	0.2041	0.0028	0.0043	13	13.5342	−0.5342	3105
31	0.1755	0.0029	0.0037	15	15.4634	−0.4634	3105
32	0.1520	0.0030	0.0032	17	17.4814	−0.4814	3105
33	0.1324	0.0031	0.0027	19	19.4891	−0.4891	3105
34	0.1156	0.0032	0.0023	21	21.3380	−0.3380	3105
35	0.1014	0.0032	0.0019	23	23.1459	−0.1459	3105
36	0.0891	0.0032	0.0017	25	24.9402	0.0598	3105
37	0.0785	0.0033	0.0014	27	26.7927	0.2073	3105
38	0.0693	0.0033	0.0012	29	28.8627	0.1373	3105
39	0.0615	0.0033	0.0010	31	30.9216	0.0784	3105
40	0.0546	0.0033	0.0009	33	33.0684	−0.0684	3105
41	0.0485	0.0033	0.0008	35	35.1807	−0.1807	3105
42	0.0432	0.0033	0.0006	37	37.2869	−0.2869	3105
43	0.0385	0.0034	0.0006	39	39.3344	−0.3344	3105
44	0.0344	0.0034	0.0005	41	41.2112	−0.2112	3105
45	0.0308	0.0034	0.0004	43	42.9103	0.0897	3105
46	0.0276	0.0034	0.0004	45	44.5651	0.4349	3105
47	0.7052	0.0013	0.0127	1	1.0867	−0.0867	5052
48	0.5319	0.0017	0.0101	3	2.9564	0.0436	5052
49	0.4277	0.0021	0.0086	5	4.9563	0.0437	5052
50	0.3545	0.0024	0.0075	7	6.7492	0.2508	5052
51	0.2988	0.0026	0.0064	9	8.7379	0.2621	5052
52	0.2546	0.0028	0.0055	11	10.8987	0.1013	5052
53	0.2189	0.0030	0.0047	13	12.8419	0.1581	5052
54	0.1894	0.0031	0.0040	15	14.7669	0.2331	5052
55	0.1647	0.0032	0.0035	17	16.8500	0.1500	5052
56	0.1440	0.0033	0.0030	19	18.9809	0.0191	5052
57	0.1264	0.0034	0.0026	21	21.0569	−0.0569	5052
58	0.1112	0.0034	0.0022	23	22.9636	0.0364	5052
59	0.0982	0.0035	0.0019	25	24.7798	0.2202	5052
60	0.0869	0.0035	0.0016	27	26.6535	0.3465	5052
61	0.0770	0.0035	0.0014	29	28.5749	0.4251	5052
62	0.0685	0.0036	0.0012	31	30.6065	0.3935	5052

Table 4. *Cont.*

Item	Total Count of Transmission Detector	Total Count of Backscatter Detector	Maximum Value of Transmission Detector	Target Outputs (mm)	Outputs of Neural Network (mm)	Error	Type of Alloy
63	0.0611	0.0036	0.0011	33	32.6834	0.3166	5052
64	0.0544	0.0036	0.0009	35	34.7513	0.2487	5052
65	0.0486	0.0036	0.0008	37	36.8039	0.1961	5052
66	0.0435	0.0036	0.0007	39	38.8587	0.1413	5052
67	0.0390	0.0036	0.0006	41	40.8243	0.1757	5052
68	0.0349	0.0036	0.0005	43	42.6907	0.3093	5052
69	0.0314	0.0036	0.0004	45	44.4360	0.5640	5052
70	0.7073	0.0013	0.0128	1	1.1634	−0.1634	6061
71	0.5343	0.0018	0.0101	3	2.9220	0.0780	6061
72	0.4301	0.0021	0.0086	5	4.8987	0.1013	6061
73	0.3568	0.0024	0.0075	7	6.6871	0.3129	6061
74	0.3009	0.0027	0.0064	9	8.6485	0.3515	6061
75	0.2564	0.0029	0.0055	11	10.8200	0.1800	6061
76	0.2206	0.0031	0.0047	13	12.7792	0.2208	6061
77	0.1909	0.0032	0.0041	15	14.7359	0.2641	6061
78	0.1660	0.0033	0.0035	17	16.8661	0.1339	6061
79	0.1452	0.0034	0.0030	19	19.0688	−0.0688	6061
80	0.1273	0.0034	0.0026	21	21.1638	−0.1638	6061
81	0.1121	0.0035	0.0023	23	23.1178	−0.1178	6061
82	0.0990	0.0035	0.0019	25	25.0342	−0.0342	6061
83	0.0875	0.0036	0.0017	27	26.8872	0.1128	6061
84	0.0776	0.0036	0.0015	29	28.8727	0.1273	6061
85	0.0690	0.0036	0.0013	31	30.8978	0.1022	6061
86	0.0614	0.0037	0.0011	33	32.9820	0.0180	6061
87	0.0548	0.0037	0.0009	35	35.0459	−0.0459	6061
88	0.0489	0.0037	0.0008	37	37.1411	−0.1411	6061
89	0.0438	0.0037	0.0007	39	39.1852	−0.1852	6061
90	0.0392	0.0037	0.0006	41	41.2230	−0.2230	6061
91	0.0352	0.0037	0.0005	43	43.1059	−0.1059	6061
92	0.0316	0.0037	0.0005	45	44.8042	0.1958	6061

The present study determined the aluminum layer thickness without regard to alloy composition. While this technique was developed for use with aluminum plates, it has broad applicability for determining the thickness of other metals. Furthermore, a neural network was unable to distinguish between various aluminum plate alloys in this study; however, future studies will be able to do so by utilizing a variety of feature extraction approaches, including time, frequency, wavelet transform, etc. To further improve the precision of the thickness detection system, it is also feasible to analyze the efficiency of several neural networks like MLP, GMDH, etc.

5. Conclusions

The purpose of this study was to introduce a technique that uses X-rays to precisely measure the thickness of aluminum plates. The structure of the proposed detection system consisted of an X-ray tube and two sodium iodide detectors. The aluminum plate with different thicknesses and four different alleles was placed in this detection system, and the recorded signals using the scattering and transmission detectors were collected and labeled. In order to reduce the volume of calculations, increase the accuracy, and better interpret the collected data, three characteristics were extracted: the total count of transmission and backscattering detectors and the maximum value of the transmission detector. Although these characteristics did not have the ability to distinguish different alloys well, they separated the thicknesses of the aluminum layer well. These characteristics were applied to the inputs of an RBF neural network to determine the thickness of aluminum. Of the 92 available samples, 64 were utilized to train the neural network, while the remaining

data were used as test data to make sure the network was working as intended. After investigating the architecture of many neural networks to determine the most accurate one, researchers discovered that an RBF neural network with 10 neurons in the hidden layer can accurately predict the value of the target parameter. The result of the neural network's performance was determining the thickness of the aluminum plate with an MRE of 2.11%, which is a very small error. In future research, the use of different neural networks and methods based on feature extraction may be on the agenda of researchers in this field, who will try to improve the structure and increase the accuracy of the detection system.

Data Availability Statement: The data presented in this study are available on request from the corresponding author.

Conflicts of Interest: The authors declare no conflict of interest.

References

1. Artem'ev, B.V.; Maslov, A.I.; Potapov, V.N.; Vedernikov, M.B. Use of X-ray thickness gauges in manufacturing rolled non-ferrous metals. *Russ. J. Nondestruct. Test.* **2003**, *39*, 459–464. [CrossRef]
2. Allport, J.J.; Nucleonic Data Systems Inc. Dual Beam X-ray Thickness Gauge. U.S. Patent 4,037,104, 1977.
3. Artemyev, I.B.; Artemiev, B.V.; Vladimirov, Y.L.; Vladimirov, L.V. Modernization of radiation detectors thickness gauge. *J. Phys. Conf. Ser.* **2017**, *808*, 012012. [CrossRef]
4. Artemiev, B.V.; Maslov, A.I. X-ray thickness gages of the Rit10 family for thickness measurement at line production of rolled metal. In Proceedings of the Abstracts of 17th World Conference on Non-Destructive Testing, Shanghai, China, 25–28 October 2008.
5. Nazemi, E.; Aminipour, M.; Olfateh, A.; Golgoun, S.M.; Davarpanah, M.R. Proposing an intelligent approach for measuring the thickness of metal sheets independent of alloy type. *Appl. Radiat. Isot.* **2019**, *149*, 65–74. [CrossRef] [PubMed]
6. Salgado, C.M.; de Freitas Dam, R.S.; de Carvalho Conti, C.; Salgado, W.L. Three-phase flow meters based on X-rays and artificial neural network to measure the flow compositions. *Flow Meas. Instrum.* **2021**, *82*, 102075. [CrossRef]
7. Remillard, R.A.; Loewenstein, M.; Steiner, J.F.; Prigozhin, G.Y.; LaMarr, B.; Enoto, T.; Gendreau, K.C.; Arzoumanian, Z.; Markwardt, C.; Basak, A.; et al. An empirical background model for the NICER X-ray timing instrument. *Astron. J.* **2022**, *163*, 130. [CrossRef]
8. Roshani, G.H.; Ali, P.J.; Mohammed, S.; Hanus, R.; Abdulkareem, L.; Alanezi, A.A.; Sattari, M.A.; Amiri, S.; Nazemi, E.; Eftekhari-Zadeh, E.; et al. Simulation study of utilizing X-ray tube in monitoring systems of liquid petroleum products. *Processes* **2021**, *9*, 828. [CrossRef]
9. Salgado, C.M.; Dam, R.S.; Salgado, W.L.; Santos, M.C.; Schirru, R. Development of a deep rectifier neural network for fluid volume fraction prediction in multiphase flows by gamma-ray densitometry. *Radiat. Phys. Chem.* **2021**, *189*, 109708. [CrossRef]
10. Pelowitz, D.B. *MCNPX User's Manual Version 2.5.0*; Los Alamos National Laboratory: Los Alamos, NM, USA, 2005; Volume 76, p. 473.
11. Pinilla, M.I. *An MCNP Simulation Study of an Oil Well Logging Benchmarking Tool and a Test Enclosure*; Kansas State University: Manhattan, KS, USA, 2019.
12. Talaat, K.; Xi, J.; Baldez, P.; Hecht, A. Radiation dosimetry of inhaled radioactive aerosols: CFPD and MCNP transport simulations of radionuclides in the lung. *Sci. Rep.* **2019**, *9*, 17450. [CrossRef]
13. Poorchitsaz, M.; Shirani Bidabadi, B.; Mohammadi, R. Investigating the Effect of Gamma Ray Source Activity on Down-hole Nuclear Density Toolâ s Reading Using Simulation by MCNP Code. *Radiat. Saf. Meas.* **2020**, *9*, 341–346.
14. Sayyed, M.I.; Mahmoud, K.A.; Tashlykov, O.L.; Khandaker, M.U.; Faruque, M.R.I. Enhancement of the Shielding Capability of Soda–Lime Glasses with Sb_2O_3 Dopant: A Potential Material for Radiation Safety in Nuclear Installations. *Appl. Sci.* **2021**, *11*, 326. [CrossRef]
15. Çağlar, M.; Karabul, Y.; Kılıç, M.; Özdemir, Z.G.; İçelli, O. $Na_2Si_3O_7$/Ag micro and nano-structured glassy composites: The experimental and MCNP simulation surveys of their radiation shielding performances. *Prog. Nucl. Energy* **2021**, *139*, 103855. [CrossRef]

16. Sun, W.; Hu, G.; Xu, H.; Li, Y.; Wang, C.; Men, T.; Ji, F.; Lao, W.; Yu, B.; Sheng, L.; et al. Study on the Influence of Reinforced Particles Spatial Arrangement on the Neutron Shielding Performance of the Composites. *Materials* **2022**, *15*, 4266. [CrossRef] [PubMed]

17. Jeong, M.; Hammig, M.D. Comparison of gamma ray localization using system matrixes obtained by either MCNP simulations or ray-driven calculations for a coded-aperture imaging system. *Nucl. Instrum. Methods Phys. Res. Sect. A Accel. Spectrometers Detect. Assoc. Equip.* **2020**, *954*, 161353. [CrossRef]

18. Jeong, M.; Kim, G. MCNP-polimi simulation for the compressed-sensing based reconstruction in a coded-aperture imaging CAI extended to partially-coded field-of-view. *Nucl. Eng. Technol.* **2021**, *53*, 199–207. [CrossRef]

19. Kerr, P.; Cherepy, N.; Church, J.; Guethlein, G.; Hall, J.; McNamee, C.; O'Neal, S.; Champley, K.; Townsend, A.; Sasagawa, M.; et al. Neutron transmission imaging with a portable DT neutron generator. *Radiat. Detect. Technol. Methods* **2022**, *6*, 234–243. [CrossRef]

20. Roshani, G.H.; Nazemi, E.; Feghhi, S.A.H. Investigation of using 60Co source and one detector for determining the flow regime and void fraction in gas–liquid twophase flows. *Flow Meas. Instrum.* **2016**, *50*, 73–79. [CrossRef]

21. Hernandez, A.M.; Boone, J.M. Tungsten anode spectral model using interpolating cubic splines: Unfiltered X-ray spectra from 20 kV to 640 kV. *Med. Phys.* **2014**, *41*, 042101. [CrossRef]

22. Sattari, M.A.; Hayati, M.; Shama, F.; Shah-Ebrahimi, S.M. A miniaturized filter design approach using GMDH neural networks. *Microw. Opt. Technol. Lett.* **2023**, *65*, 2507–2516. [CrossRef]

23. Taylan, O.; Sattari, M.A.; Elhachfi Essoussi, I.; Nazemi, E. Frequency domain feature extraction investigation to increase the accuracy of an intelligent nondestructive system for volume fraction and regime determination of gas-water-oil three-phase flows. *Mathematics* **2021**, *9*, 2091. [CrossRef]

24. Alamoudi, M.; Sattari, M.A.; Balubaid, M.; Eftekhari-Zadeh, E.; Nazemi, E.; Taylan, O.; Kalmoun, E.M. Application of gamma attenuation technique and artificial intelligence to detect scale thickness in pipelines in which two-phase flows with different flow regimes and void fractions exist. *Symmetry* **2021**, *13*, 1198. [CrossRef]

25. Maraveas, C.; Bartzanas, T. Sensors for structural health monitoring of agricultural structures. *Sensors* **2021**, *21*, 314. [CrossRef] [PubMed]

26. Maraveas, C.; Asteris, P.G.; Arvanitis, K.G.; Bartzanas, T.; Loukatos, D. Application of bio and nature-inspired algorithms in agricultural engineering. *Arch. Comput. Methods Eng.* **2023**, *30*, 1979–2012. [CrossRef]

27. Hartman, E.J.; Keeler, J.D.; Kowalski, J.M. Layered neural networks with Gaussian hidden units as universal approxima-tors. *Neural Comput.* **1990**, *2*, 210–215. [CrossRef]

28. Zhang, Q.; Guo, L.; Sohan, M.A.H.; Tian, X. Research on the Control Problem of Autonomous Underwater Vehicles Based on Strongly Coupled Radial Basis Function Conditions. *Appl. Sci.* **2023**, *13*, 7732. [CrossRef]

29. Szwajka, K.; Zielińska-Szwajka, J.; Trzepieciński, T. The Use of a Radial Basis Function Neural Network and Fuzzy Modelling in the Assessment of Surface Roughness in the MDF Milling Process. *Materials* **2023**, *16*, 5292. [CrossRef]

30. Ralambondrainy, H. A conceptual version of the k-means algorithm. *Pattern Recognit. Lett.* **1995**, *16*, 1147–1157. [CrossRef]

31. Cottrell, M.; Rousset, P. The Kohonen algorithm: A powerful tool for analysing and representing multidimensional quantitative and qualitative data. In *International Work-Conference on Artificial Neural Networks*; Springer: Berlin/Heidelberg, Germany, 1997; pp. 861–871.